Interaction of Pions with Complex Nuclei

DONALD HARVEY STORK
Radiation Laboratory, Department of Physics, University of California, Berkeley, California
(Received November 12, 1953)

Attenuation cross sections and cross sections for scattering into a fixed angular interval have been measured in a well-defined geometry for pions of energies 33, 46, and 68 Mev. The targets were beryllium, carbon, aluminum, and copper. The results were analyzed by means of the optical model, and a strong energy dependence was found for the pion interaction mean free path in nuclear matter. A satisfactory representation of this energy dependence is the equation

$$\lambda_a/r_0=[2b(kr_0)^4/\gamma^2]^{-1},$$

where λ_a is the mean free path, r_0 is the pion Compton wavelength, b is a constant, k is the pion number, and γ is the total pion energy divided by its rest energy. The results of an optical model calculation with the above energy dependence were compared with other published pion-nucleus data and agreement was found. A partial wave analysis gave essentially the same results but required mean free paths about twice as long.

Published values of the pion-nucleon phase shifts at several energies were used to calculate the mean free path by means of multiple-scattering theory. The results agree with the above energy dependence and are intermediate between the mean free paths of the optical model and those of the partial wave analysis.

INTRODUCTION

THE total cross section for pions in complex nuclei may be considered to consist of two parts: an elastic (coherent) scattering cross section, σ_s, and an interaction cross section, σ_a. The latter includes all processes—such as star formation, inelastic scattering, and charge-exchange scattering—that remove pions from the coherent wave. If a model is adopted in which the pion-nucleus interaction is represented by a complex square well, of depth V_r+iV_i and of radius R, an experimental measurement of σ_s and σ_a permits determination of the depth of this complex well. It is expected that the variation of the well depth with pion energy should reflect the characteristics of the pion-nucleon interaction.

The first experiments employing artificially produced pions for the study of pion cross sections in complex nuclei were performed by observation of the interactions occurring along both positive and negative pion tracks in nuclear emulsions.[1–3] A number of pion energies between 30 and 100 Mev were used. The study was extended to pure carbon targets in cloud-chamber experiments for 48-Mev[4] and 62-Mev[5] positive and negative pions. In addition to the total cross-section measurements, the above experiments gave further information, such as the star-prong distributions and the inelastic and elastic scattering distributions. Tracy[6] has recently made a cloud-chamber study of the pion interaction in aluminum at several energies. Measurements of the attenuation of negative pions as a function of A have been made by Chedester *et al.*[7] at 85 Mev and by Martin[8] at 113 and 137 Mev. In the latter case the results were analyzed to give the interaction cross section, σ_a.

The attenuation and scattering experiment described in this paper is intended to provide further pion-nucleus cross-section data at relatively low energies and thus to make possible a better understanding of the behavior of the pion-nucleus interaction.

EXPERIMENTAL PROCEDURE

Three pion energies were chosen for this study: 33, 46, and 68 Mev. The target nuclei were beryllium, carbon, aluminum, and copper. For the purpose of distinguishing the pions from the background, a momentum selection and a pulse-height analysis were made. The attenuation cross sections for the various targets at the three pion energies were measured in a well-defined geometry. The cross sections for pion scattering into a fixed angular interval were obtained simultaneously.

The general physical arrangement for the experiment is shown in Fig. 1. The pion beams were produced by bombarding either a polyethylene or a carbon production target by the 340-Mev external scattered proton beam at the 184-inch synchrocyclotron. The target was placed in the 5-inch gap of a large pair spectrometer magnet. Pions produced in the forward direction were bent through an arc of 90° in an 18.5-inch radius, leaving the magnet gap through a brass slit in a direction 35° to the normal of the magnetic field boundary. The pions continued through a hole in the 5-foot-thick concrete shielding, passed through a collimating counter inside the shielding, and entered the main counting

[1] Bernardini, Booth, and Lederman, Phys. Rev. **83**, 1075 and 1277 (1951).
[2] G. Bernardini and F. Levy, Phys. Rev. **84**, 610 (1951).
[3] H. Bradner and B. Rankin, Phys. Rev. **87**, 547 and 553 (1952).
[4] A. M. Shapiro, Phys. Rev. **84**, 1063 (1951).
[5] Byfield, Kessler, and Lederman, Phys. Rev. **86**, 17 (1952).
[6] J. Tracy, Phys. Rev. **91**, 960 (1953).
[7] Chedester, Isaacs, Sachs, and Steinberger, Phys. Rev. **82**, 958 (1951).
[8] R. Martin, Phys. Rev. **87**, 1052 (1952).

system just outside the shielding. The geometry was such that because of the properties of the fringing field at the exit of the magnet gap, a first-order focus of the pion beam in the vertical plane was obtained. Thus, in the vertical plane, a pion image of the proton beam at the production target was formed at the counter system. This focusing effect was verified experimentally by observation of the counting rate as the magnet was raised and lowered.

For the 33- and 46-Mev cross-section measurements, a polyethylene $[(CH_2)_n]$ target was used to produce the beam pions. Advantage was taken of the large cross section for the reaction $p+p\rightarrow\pi^++d$,[9] from which monoenergetic pions are obtained in the forward direction for a given incident proton energy. The energy of these pions upon emerging from the target depends upon the thickness of the target but is essentially independent of the target depth at which they are produced.[10] Thus the polyethylene target provided monoenergetic positive pion beams whose energy could be varied by changing the target thickness (the magnetic field being adjusted to maximize the pion flux). For the 68-Mev cross-section measurements, the required pion beam energy was too high to be obtained from the reaction $p+p\rightarrow\pi^++d$. In this case a 2-inch carbon production target was used. For protons incident upon carbon, positive pions are produced over a broad energy spectrum.[11] Consequently, the value of the magnetic field was set to bend pions of the appropriate energy through the field exit and in the direction of the counting system.

The pion energy distributions for the three beams were determined by range in copper with a pulse-height selection that is described below. The energy was measured before and after each experimental run, and in no case was a significant change in energy found. As the pions entered the attenuation target, after passing through the collimating, pulse-height, and passing counters (Fig. 1), the three pion beams had mean energies and half-widths at half-maximum of 37.5±4, 51±3, and 73±8 Mev. For the two lower energies, most of the beam pions were from the reaction $p+p\rightarrow\pi^++d$, and the energy distributions were somewhat narrower than that defined solely by the momentum selection. For the pion beam of higher energy, from the carbon production target, the energy distribution was determined almost entirely by the momentum selection. The momentum selection in turn was determined by the positions and widths of the production target, field exit slit, and counters.

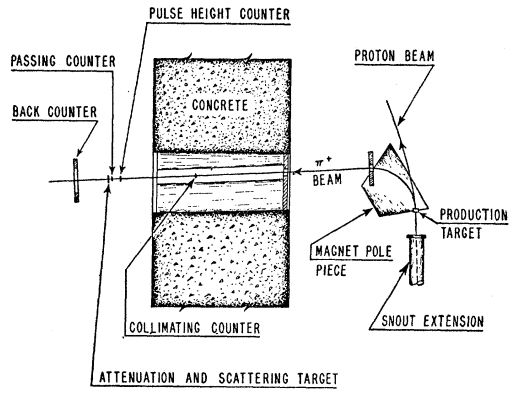

FIG. 1. Physical arrangement.

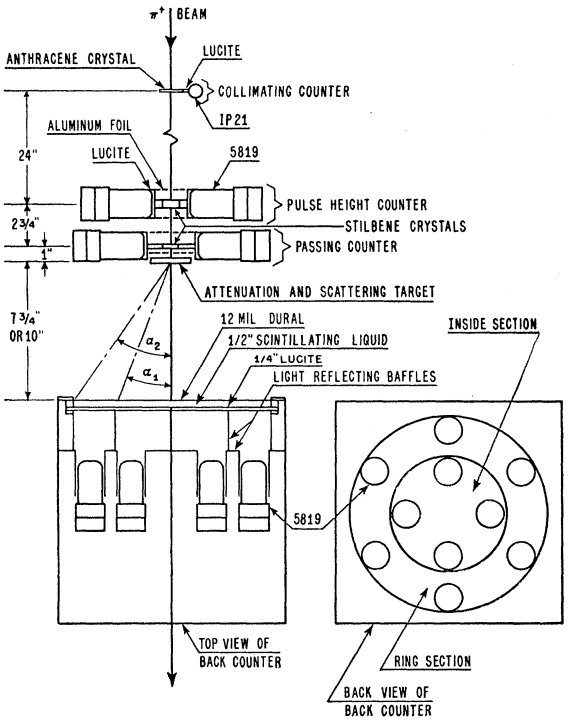

FIG. 2. Counter system and geometry.

The pion beam flux at the counter system varied between one and two pions per square inch per second. This low flux required an efficient method of taking data. Such a method was found in the photographic-recording method described below.

The geometry of the counter system is shown in Fig. 2. The first ("collimating") counter consisted of a $\frac{1}{8}$-inch thick, $1\frac{1}{2}$-inch square anthracene crystal viewed through a short Lucite light pipe by a 1P21 photomultiplier. The second ("pulse-height") counter consisted of a $\frac{1}{2}$-inch thick, $1\frac{1}{4}$-inch square stilbene crystal viewed on two sides through short Lucite light pipes by 5819 photomultipliers. Short signal leads from the two 5819's were connected together at a coaxial tee, and the tubes were matched in gain by suitably adjusting their voltages. The third counter was a "passing" counter, similar in construction to the pulse-

[9] Cartwright, Richman, Whitehead, and Wilcox, Phys. Rev. **91**, 677 (1953).
[10] Richman, Skinner, Merritt, and Youtz, Phys. Rev. **80**, 900 (1950).
[11] W. Dudziak (private communication).

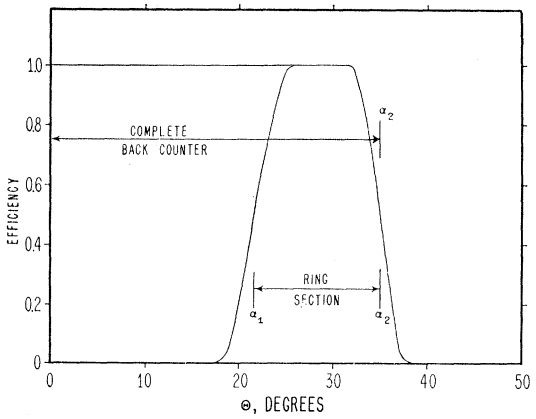

FIG. 3. Angular efficiency of the back counter.

height counter. The crystal was stilbene, $\frac{1}{4}$ inch thick and $1\frac{3}{16}$ inches square. Immediately following the passing counter was the attenuation and scattering target.

Behind the target was the back counter, whose sensitive volume consisted of a disk-shaped liquid scintillator 14 inches in diameter. The solution was terphenyl in phenylcyclohexane with the "red shifter," diphenylhexatriene, added. The scintillator was divided into two sections by means of aluminum-foil light reflectors placed behind the Lucite back face. By means of this division an inner 8-inch diameter circle was viewed by four 5819 photomultipliers, and an outer 3-inch ring was viewed by six 5819 photomultipliers. Signal leads from the inner four 5819's were connected together to a single coaxial connecter, and leads from the outer six 5819's were connected together to a second coaxial connecter. In this way separate signals from the two sections of the back counter could be obtained. The gains of the tubes were matched by suitably adjusting their individual voltages. The response across the face of the back counter was found to be uniform to about 10 percent. The fraction of statistically zero pulses caused by fluctuations in the number of photoelectrons collected for each pulse was determined to be negligibly small.

Because of the overlap in light collection, the full 14-inch diameter could be used, with no blind spots, for attenuation measurements. Particles passing through the scintillator near the division between the inner and outer sections gave rise to a pulse from both sections. However, by the establishment of a pulse-height criterion for distinguishing through which side of the division a particle passed, the separation became satisfactorily distinct. In this way the back counter was made suitable for the simultaneous measurement of the attenuation cross section and of the cross section for scattering into a fixed angular interval.

An attenuation event was defined as an event in which a particle that passed through the front three counters failed to reach either section of the back counter. A ring-counter (scattering) event was defined as one in which a particle traversed the front three counters and appeared to pass through the ring section of the back counter, the pulse-height criterion's being used if pulses from both the inside and outside sections of the back counter were present. Since the pion beam was of finite extent, it was required that the back counter be large enough for the geometry to be well defined. The angular efficiency of the back counter as a whole and of the ring-counter section is shown in Fig. 3 for a 10-inch separation from the target to the back counter. For this separation, the two sections of the back counter subtended half-angles with respect to the target of 21.7° (α_1) and 35° (α_2) (see Fig. 2). For Al and Cu targets at low energy, multiple Coulomb scattering necessitated thinner targets and greater angles. The back counter was then placed $7\frac{3}{4}$ inches from the target, giving $\alpha_1=26.6°$ and $\alpha_2=42°$.

A block diagram of the electronics is shown in Fig. 4. If a particle passed through the front three counters, a coincidence was formed and the coincidence output triggered the oscilloscope sweep. Pulses from the pulse-height counter, the passing counter, and from either section of the back counter, if present, appeared on the oscilloscope trace. A separation of the pulses on the trace was accomplished by means of the different lengths of *RG65/U* delay line.

The oscilloscope traces were photographed on continuously moving Kodak Linagraph Pan 35-mm film by means of a General Radio camera. Upon completion of a run, the film was processed and the images of the oscilloscope traces were examined in a Recordak microfilm viewer. The position and height of each pulse

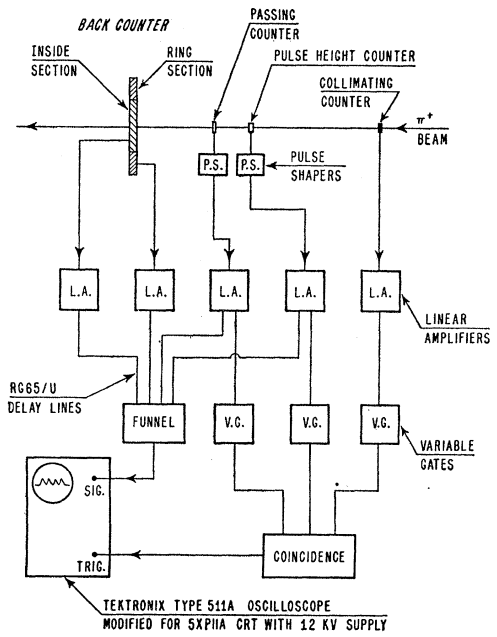

FIG. 4. Block diagram of the electronics.

appearing on the traces could be conveniently measured by projecting the image on ordinary graph paper. A sample strip of the film is reproduced in Fig. 5. The time separation of the pulses, obtained by the different lengths of delay line used for each signal, was about 0.8 microsecond. Measurement of the separation of the pulses could be converted to a time measurement, and separation of the starting points of the pulses could be readily determined to within 0.04 microsecond. This was considered the effective resolving time for determining coincidences. The pulse heights were measured on a scale of one hundred divisions on which a reading resolution of one division could be obtained.

The principal use of pulse-height measurements was to aid in the separation of the pions from the background. For this purpose the relative heights of the pulses from the pulse-height counter were measured. The pulse-height distribution for the total beam flux was determined in a random sampling of the traces on the film. (The solid curve in Fig. 6 represents the pulse-height distribution of the beam flux at 46 Mev. The distributions at 33 and 68 Mev are similar.) A peak in the pulse-height distribution (of about 20 percent full-width at half-maximum) was caused by the pions in the beam. The pulse-height resolution was sufficiently narrow to distinguish the pions from electrons. The largest background was found in the large-pulse region and was well separated from the pion pulse height. The number of pions passing through the target was thus determined by multiplication of the total

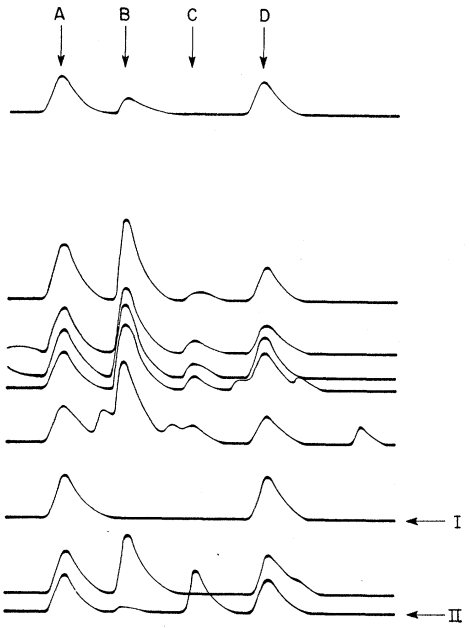

FIG. 5. Reproduction of the traces on a sample strip of film. Pulse A is from the pulse-height counter, pulse B is from the inside section of the back counter, pulse C—when present—is from the ring section of the back counter, and pulse D is from the passing counter. Traces I and II correspond to an attenuation event and a ring-counter event, respectively.

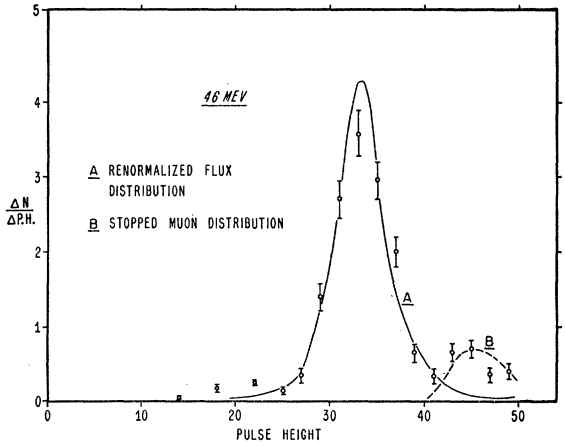

FIG. 6. Pulse-height distribution of attenuation events.

number of photographed oscilloscope traces by the fraction of traces for which the pulse height was inside the narrow pulse-height band representing the pions.

The number of events was determined by examining each image of the oscilloscope traces. In an attenuation event (trace I in Fig. 5), there was no pulse from either section of the back counter. In a ring-counter event (trace II in Fig. 5), there was a pulse from the ring section but not from the inside section of the back counter, or—if the particle passed near the division between the two sections of the back counter—the pulse from the ring section was larger and that from the inside section smaller than a predetermined pulse height. For every event the pulse height was measured, and the same pulse-height selection that was used for the total number of pions was applied to the events. (The pulse-height distribution of the attenuation events is shown in Fig. 6 for the 46-Mev measurements.) All events in which the pulse height fell outside the narrow pion pulse-height band were discarded.

From the total number of pions and of events, both selected on the basis of pulse height, the fraction of the pions causing events was calculated. Runs were made with the target in and with the target removed. A subtraction gave the fraction of pions causing events in the target. After the corrections described below were made, the attenuation and ring-counter cross sections per target nucleus were computed using the equation $f=\exp(-N\sigma x)$, where f is the fraction of pions causing events, N the number of target nuclei per gram, σ the cross section in cm^2, and x the thickness of the target in grams/cm^2.

CORRECTIONS

A. Accidentals

The number of accidental coincidences triggering the oscilloscope sweep was negligible. Accidental single pulses, however, appeared fairly frequently on the oscilloscope traces. (Several of these accidental pulses

TABLE I. The measured attenuation cross sections.

Pion energy, Mev	α_2	Target	Target thickness g/cm²	Fraction of pions attenuated[a] (times 100)	Correction fraction (times 100) Accidentals	Decay muons	$\sigma_m/\pi R^2$	$1+V_c/T_\pi$	$\sigma_m\left(1+\frac{V_c}{T_\pi}\right)\Big/\pi R^2$
33±6	35°	Be	2.587	1.88±0.20	+0.07	−0.27	0.366±0.044	1.058	0.387±0.047
33±6	35	C	2.555	1.84±0.21	+0.07	−0.30	0.389±0.050	1.079	0.420±0.054
33±5	42	Al	2.012	1.25±0.19	+0.07	−0.21	0.456±0.088	1.131	0.515±0.099
33±5	42	Cu	2.342	1.20±0.19	+0.07	−0.21	0.486±0.090	1.220	0.593±0.105
46±6	35	Be	3.452	2.93±0.27	+0.07	−0.14	0.473±0.044	1.042	0.492±0.046
46±6	35	C	3.232	3.05±0.27	+0.08	−0.17	0.570±0.052	1.057	0.603±0.055
46±6	35	Al	3.826	3.21±0.28	+0.07	−0.17	0.666±0.058	1.094	0.730±0.064
46±6	35	Cu	4.224	2.45±0.25	+0.08	−0.17	0.606±0.064	1.158	0.702±0.074
68±10	35	Be	4.601	5.28±0.32	+0.19	−0.01	0.684±0.041	1.028	0.703±0.042
68±10	35	C	4.190	4.46±0.30	+0.17	−0.01	0.695±0.046	1.038	0.722±0.048
68±10	35	Al	4.748	4.75±0.32	+0.16	−0.02	0.840±0.055	1.064	0.903±0.059
68±10	35	Cu	5.620	4.20±0.31	+0.15	−0.02	0.847±0.061	1.107	0.938±0.068

[a] Corrected for 4 percent muon-flux contamination.

may be seen in Fig. 5.) If an accidental pulse had appeared at the position of the pulse from either section of the back counter in the case of an event, the event would have been misinterpreted or missed. Consequently, it was necessary to determine the accidental-pulse frequency and pulse-height distribution for each section of the film in order to correct for the effect of these spurious pulses. The corrections are shown in Tables I and II.

B. Pion-Muon Decay

The presence in the beam of muons originating from the decay of pions in flight required a correction to both the flux and the number of events. The muons from decay in flight were carried forward from the point of decay, by the center-of-mass motion, within a narrow cone with the maximum laboratory decay angle depending upon the pion energy. The laboratory energy of the muons varied widely. Where the decay occurred before the pulse-height counter and passed through the counter system, some of the low-energy muons could be distinguished from the beam pions by the pulse-height selection.

The correction for the muon flux through the target was determined by range measurements. Most of the decay muons had ranges greater than that of the pions. From the number of long-range particles present in the beam it was estimated that about 4 percent of the pulse-height selected particles in the beam were muons. It was assumed that the muons did not interact in the target, and a 4 percent correction was made to the beam flux.

A correction to the number of attenuation events was required because of the presence of decay muons having such low energy that they came to the end of their range in the target. Such occurrences appeared as attenuation events, for there were no pulses from the back counter. The pulse-height selection eliminated these spurious events if the decays occurred before the pions reached the pulse-height counter. (Such events are found in the excess of large pulses just above the pion pulse-height peak in Fig. 6.) However, for low-

TABLE II. The measured ring-counter cross sections.

Pion energy, Mev	α_1	α_2	Target	Target thickness g/cm²	Fraction of pions causing ring counter events[a] (times 100)	Correction fraction (times 100) Accidentals	Decay muons	Mult. Coul. scat.	$\Delta\sigma_m/\pi R^2$	$1+\frac{V_c}{T_\pi}$	$\Delta\sigma_m\left(1+\frac{V_c}{T_\pi}\right)\Big/\pi R^2$
33±6	21.7°	35°	Be	2.587	0.32±0.14	−0.03	−0.14	−0.00	0.031±0.030	1.058	0.032±0.031
33±6	21.7	35	C	2.555	0.55±0.15	−0.03	−0.18	−0.02	0.074±0.034	1.079	0.081±0.037
33±6	21.7	35	Al	2.704	1.13±0.25	−0.01	−0.23	−0.41	0.137±0.071	1.131	0.155±0.080[b]
33±5	26.6	42	Al	2.012	0.40±0.13	−0.03	−0.14	−0.00	0.085±0.045	1.131	0.096±0.051
33±6	21.7	35	Cu	3.242	4.90±0.60	−0.01	−0.29	−4.42	0.038±0.165	1.220	0.046±0.201[b]
33±5	26.6	42	Cu	2.342	0.91±0.16	−0.06	−0.22	−0.40	0.090±0.060	1.220	0.110±0.073
46±6	21.7	35	Be	3.452	0.27±0.13	−0.03	−0.06	−0.00	0.027±0.021	1.042	0.028±0.022
46±6	21.7	35	C	3.232	0.45±0.15	−0.03	−0.09	−0.00	0.061±0.026	1.057	0.065±0.028
46±6	21.7	35	Al	3.826	1.02±0.18	−0.03	−0.20	−0.08	0.148±0.034	1.094	0.161±0.037
46±6	21.7	35	Cu	4.224	1.24±0.17	−0.03	−0.30	−1.66	(−0.23 ±0.05)	1.158	···[b]
68±10	21.7	35	Be	4.601	0.65±0.17	−0.07	−0.00	−0.00	0.071±0.020	1.028	0.073±0.021
68±10	21.7	35	C	4.190	0.64±0.18	−0.06	−0.00	−0.00	0.084±0.026	1.038	0.087±0.026
68±10	21.7	35	Al	4.748	0.92±0.18	−0.06	−0.00	−0.00	0.146±0.029	1.064	0.155±0.031
68±10	21.7	35	Cu	5.620	1.04±0.18	−0.06	−0.00	−0.36	0.105±0.020	1.107	0.116±0.035[b]

[a] Corrected for 4 percent muon-flux contamination.
[b] Omitted from analysis because of uncertainty in multiple-Coulomb-scattering correction.

energy muons arising from pion decays between the pulse-height counter and the target and stopping in the latter, it was necessary to derive a correction analytically (basing the derivation on the geometry, the stopping power of the counters and targets, and the pion-muon decay lifetime and kinematics). The correction is shown in Table I for each measurement.

Similarly, a correction to the number of ring-counter events was required because of decay muons that passed through the ring counter. The angular distribution of the decay muons was peaked near the maximum laboratory decay angle. Since the maximum decay angle was generally close to α_1 (see Fig. 2), it was necessary to take into account the multiple Coulomb scattering of the pions and muons in the crystals and target. The correction was derived by means of a graphical analysis and was based upon the pion-muon decay lifetime and kinematics, geometry and stopping power, and multiple Coulomb scattering. This correction can be traced to three effects: first, the increased multiple Coulomb scattering with the target in position; second, the stopping in the target of some muons that would have reached the ring counter in the absence of the target; and third, the decreased energy of pions after passing through the target and the subsequent increase in maximum pion-muon decay angle. The correction for each measurement is shown in Table II. In several cases the correction was comparable to the statistical uncertainty of the measurement. The correction, however, is considered to be of sufficient accuracy for its uncertainty to be small compared with the statistical uncertainty.

C. Multiple Coulomb Scattering

The distribution in angle of multiple Coulomb scattering was taken to be Gaussian. The Rossi and Greisen[12] expression for the mean-square angular deviation was used with the nuclear radius substituted for the minimum impact parameter. It was found that the contribution of large-angle multiple Coulomb scattering to the measured attenuation cross section was negligible. For the ring-counter cross section, however, a significent correction was required in several cases to account for pions that passed through the ring counter because of multiple Coulomb scattering in the front counters and target. The correction for each ring-counter measurement is given in Table II.

For Cu and Al at 33 Mev, two target thicknesses and back-counter angles were chosen in order empirically to determine the effect of multiple Coulomb scattering. With the thicker Cu target, the ring-counter effect was almost entirely due to multiple Coulomb scattering (see Table II); the agreement between the corrected cross sections for the two Cu thicknesses was thus interpreted as a satisfactory test of the validity of the multiple Coulomb scattering correction at this energy. At 46 Mev, however, the multiple-Coulomb-scattering correction for Cu was vastly overestimated, and led to a negative cross section (Table II). Because of this large discrepancy, the Cu ring-counter cross sections at both 46 and 68 Mev were discarded and were not considered in the analysis that follows below. Except for the cases noted above, the correction for multiple Coulomb scattering was significantly smaller than the statistical uncertainty of the measurement.

[12] B. Rossi and K. Greisen, Revs. Modern Phys. **13**, 263 (1941).

EXPERIMENTAL RESULTS

The data and results for the attenuation cross sections are given in Table I. The pion energies listed are the mean energies of the pion beams in the targets, and the energy spread is that caused by the energy width of the beam and by the energy loss in the targets. The uncertainties shown for the fraction of pions attenuated and for the resulting cross sections are statistical standard deviations. The measured attenuation cross section divided by nuclear area is denoted by $\sigma_m/\pi R^2$. The nuclear area was taken to be πR^2, where $R=r_0A^{\frac{1}{3}}$. A is the atomic mass number, and $r_0=\hbar/m_\pi c=1.4\times10^{-13}$ cm.

For the analysis that follows, it was desired to remove the effects due to Coulomb suppression of the positively charged pion wave function at the nucleus. A correction factor,[5] $1+V_c/T_\pi$, may be derived by use of the classical-particle picture for Coulomb scattering, for the purpose of determining the impact parameter for a pion passing at a distance R from the center of the nucleus. This impact parameter is then considered to be the effective nuclear radius. V_c is the Coulomb potential at R and T_π is the pion kinetic energy. Values for the correction factor and for the corrected cross section divided by nuclear area are given in the last two columns of Table I.

Similar information is listed for the ring-counter cross section in Table II, wherein α_1 and α_2 refer to the half-angles subtended by the two boundaries of the back counter (see Fig. 2). The measured ring-counter cross section is designated $\Delta\sigma_m$. Except for the cases that were discarded because of the uncertainty in the multiple-Coulomb-scattering correction, the systematic errors were estimated to be small compared to the statistical standard deviations for both the ring counter and the attenuation cross sections.

ANALYSIS OF THE DATA

Because of the unique geometry used in the experiment, the measured cross sections could not readily be interpreted in themselves, and a model was required for the analysis of their various components. A model was chosen in which the nuclear interaction potential is represented by a complex square well, V_r+iV_i, of radius R. This complex square well is the basis of the optical model of Fernbach, Serber, and Taylor.[13] It

[13] Fernbach, Serber, and Taylor, Phys. Rev. **75**, 1352 (1949).

has been used in connection with the optical model by Bethe and Wilson[14] in a discussion of the 48-Mev pion-carbon interaction results of Shapiro.[4] It has also been used in connection with a partial wave analysis by Byfield *et al.*[5] in an analysis of their results for the pion-carbon interaction at 62 Mev.

A plane wave amplitude outside the square well may be written with the spatial dependence e^{ikx}, where $k=p_\pi/\hbar$ is the outside wave number and p_π is the initial pion momentum. Inside the square well the plane wave amplitude may be written as $e^{ik'x}$, where

$$k'=k+k_1+ik_2=p_\pi'/\hbar \qquad (1)$$

is the wave number inside. Here p_π' is the complex momentum of the pion inside the square well; although the analysis was implicitly based on the Schrödinger wave equation, relativistic momenta were used throughout in deriving the wave numbers. Here k_1 is the difference between the real part of the inside wave number and the outside wave number; k_2 is the imaginary part of the inside wave number.

Two cross sections result from this model: an elastic-scattering (coherent) cross section, σ_s, and an interaction cross section, σ_a. The latter includes all incoherent processes such as absorption or star formation, inelastic scattering, and charge exchange scattering. The amplitude of a plane wave inside the square well contains the term e^{-k_2x}. This decrease in amplitude is interpreted as the removal of pions from the coherent wave, and k_2 may be expected to be directly related to the interaction cross section. The coherent scattering cross section is strictly a wave phenomenon and will depend upon both k_1 and k_2. Hereafter, k_1 and k_2, rather than the complex square well, will be considered as the parameters of the analysis and will be written and evaluated as k_1r_0 and k_2r_0.

The cross sections measured in this experiment may be written in terms of σ_s and σ_a. The measured attenuation cross section includes all of σ_a except for a small fraction of cases in which an ionizing particle from the interaction passed through the back counter. It also includes all elastic scattering for angles greater than α_2 (see Fig. 2). The measured attenuation cross section may therefore be written as

$$\sigma_m=F_a\sigma_a+F_\alpha\sigma_s, \qquad (2)$$

where F_a is the fraction of the interaction cross section included in the measurement and F_α is the fraction of the total elastic scattering cross section for angles greater than α_2. The ring-counter cross section included primarily the elastic scattering for angles between α_1 and α_2 and a small contribution due to ionizing particles from interaction events. Single Coulomb scattering also contributed to the ring-counter cross section, as did the interference between the nuclear and the Coulomb scattering. The measured ring-counter cross section may therefore be written as

$$\Delta\sigma_m=\Delta F_a\sigma_a+\Delta F_\alpha\sigma_s+\Delta\sigma_{\text{Coul.}}+\Delta\sigma_{\text{interf.}}, \qquad (3)$$

where ΔF_a and ΔF_α are the fractions of interaction and scattering events reaching the ring counter.

The purpose of the analysis was to find a unique pair of parameters k_1r_0 and k_2r_0, at each energy, that would provide a best fit to both the measured attenuation and ring-counter cross sections. The various contributions to Eqs. (2) and (3) were determined by the following methods: (1) σ_a, σ_s, F_α, and ΔF_α were calculated by means of the optical model; (2) $\Delta\sigma_{\text{Coul.}}$ and $\Delta\sigma_{\text{interf.}}$ were determined by means of the Born approximation; (3) F_a and ΔF_a were estimated from the results of other experiments.

(1) Although an exact solution for σ_a and σ_s may be obtained for the complex square well by means of a partial wave analysis, calculation of the required phase shifts as a function of the two arbitrary parameters k_1r_0 and k_2r_0 for each nucleus and pion energy was found to be excessively time-consuming and was beyond the scope of this paper. Consequently, the approximate derivation of σ_a and σ_s by the optical model of Fernbach, Serber, and Taylor[13] was used. The approximation in the optical model is the neglecting of reflection and refraction of the incident wave at the boundary of the nucleus. The scattering angular distribution is also given in reference 13. From this, there could be derived the fraction scattered through angles greater than α_2, F_α, and the fraction scattered into the ring counter, ΔF_α. This was done for several different pairs of parameters, k_1r_0 and k_2r_0, with the result that these fractions were found to be independent of k_1r_0 and k_2r_0 and were a function only of kR.

(2) The Coulomb scattering and Coulomb interference were calculated by means of the Born approximation. The potential was taken to be the screened Coulomb potential of a uniformly charged sphere of radius R and with charge Ze, in addition to the complex well V_r+iV_i, also of radius R. It was found that the contribution from the square well alone gave the same scattering angular distribution as the optical model. The magnitude of the scattering, however, was larger for the Born approximation than for the optical model. For small k_1r_0 and k_2r_0, the two models gave equal scattering, but if either parameter became large, that is, if there was appreciable disturbance of the incident wave, the discrepancy between the Born approximation

TABLE III. Parameters for the best fit to the measured cross sections.

T_π, Mev	k_1r_0	k_2r_0
33	$0.18^{+0.03}_{-0.04}$	$0.04^{+0.03}_{-0.02}$
46	$0.26^{+0.03}_{-0.05}$	$0.03^{+0.04}_{-0.03}$
68	$0.17^{+0.05}_{-0.13}$	$0.17^{+0.05}_{-0.04}$

[14] H. A. Bethe and P. R. Wilson, Phys. Rev. **83**, 690 (1951).

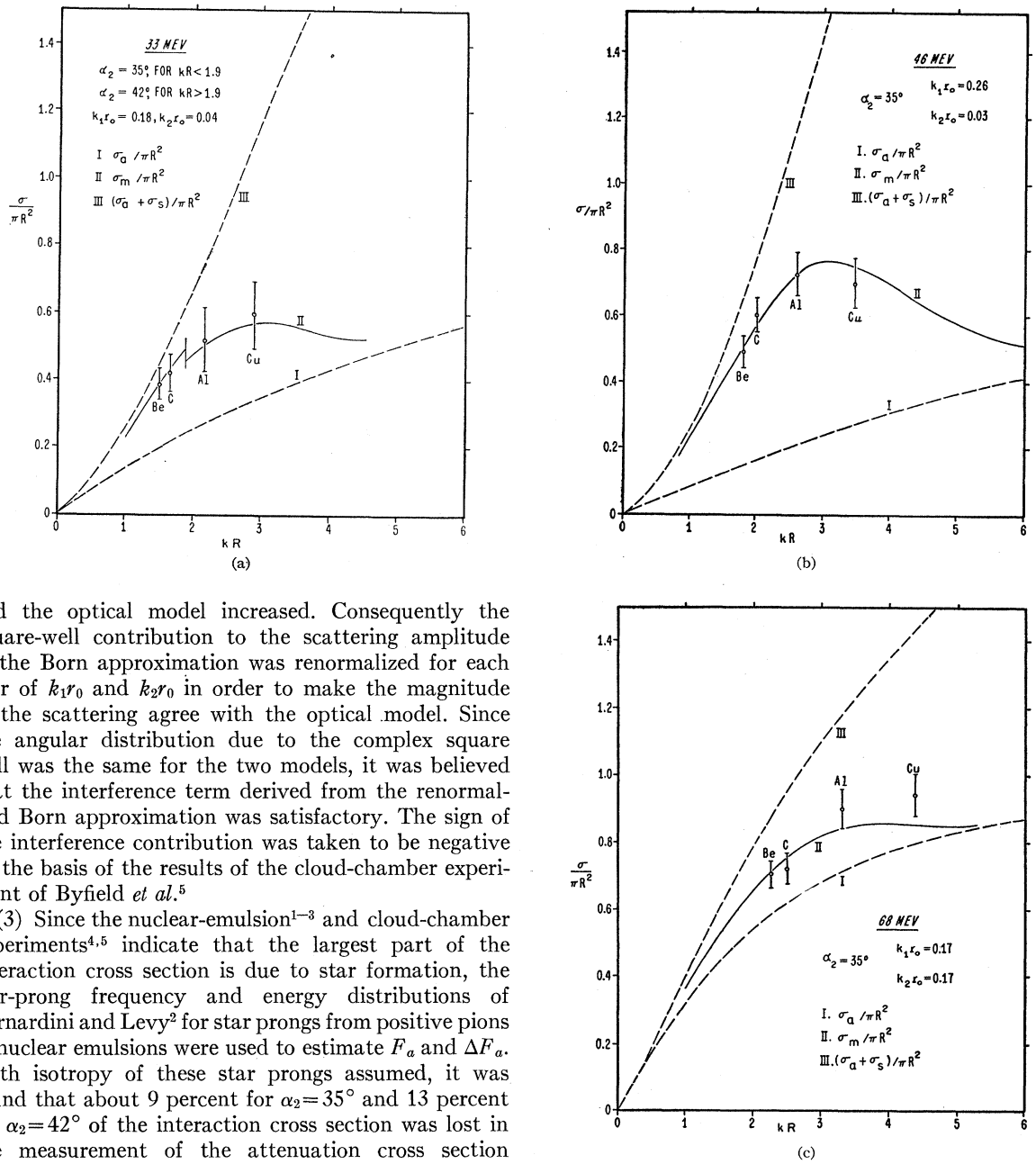

FIG. 7. The measured attenuation cross sections. The solid curve represents Eq. (2).

and the optical model increased. Consequently the square-well contribution to the scattering amplitude in the Born approximation was renormalized for each pair of k_1r_0 and k_2r_0 in order to make the magnitude of the scattering agree with the optical model. Since the angular distribution due to the complex square well was the same for the two models, it was believed that the interference term derived from the renormalized Born approximation was satisfactory. The sign of the interference contribution was taken to be negative on the basis of the results of the cloud-chamber experiment of Byfield *et al.*[5]

(3) Since the nuclear-emulsion[1–3] and cloud-chamber experiments[4,5] indicate that the largest part of the interaction cross section is due to star formation, the star-prong frequency and energy distributions of Bernardini and Levy[2] for star prongs from positive pions in nuclear emulsions were used to estimate F_a and ΔF_a. With isotropy of these star prongs assumed, it was found that about 9 percent for $\alpha_2=35°$ and 13 percent for $\alpha_2=42°$ of the interaction cross section was lost in the measurement of the attenuation cross section because of star prongs reaching the back counter. Consequently, F_a was taken to be 0.91 and 0.87 for the two geometries. Similarly, for the ring-counter cross sections, ΔF_a was found to be 0.05 for the smaller angle geometry and 0.07 for the larger angle geometry. Although these calculations are subject to serious question, the relative contribution of the star prongs was small.

By means of the above methods, σ_m and $\Delta\sigma_m$ were computed according to Eqs. (2) and (3) as a function of the two arbitrary parameters k_1r_0 and k_2r_0 for each target nucleus and pion energy. For each of the three pion energies a graphical analysis was performed to determine the values of k_1r_0 and k_2r_0 giving a best fit of Eqs. (2) and (3) to the several measured cross sections. The results are listed in Table III.

For the best-fit values of the parameters, attenuation cross sections, calculated according to Eq. (2), are plotted *versus* the dimensionless quantity kR in Fig. 7 for the three pion energies. Also shown are the measured cross sections corrected by the factor $1+V_c/T_\pi$. (The Born approximation treatment of the Coulomb scattering in the analysis is a first-order effect. The sup-

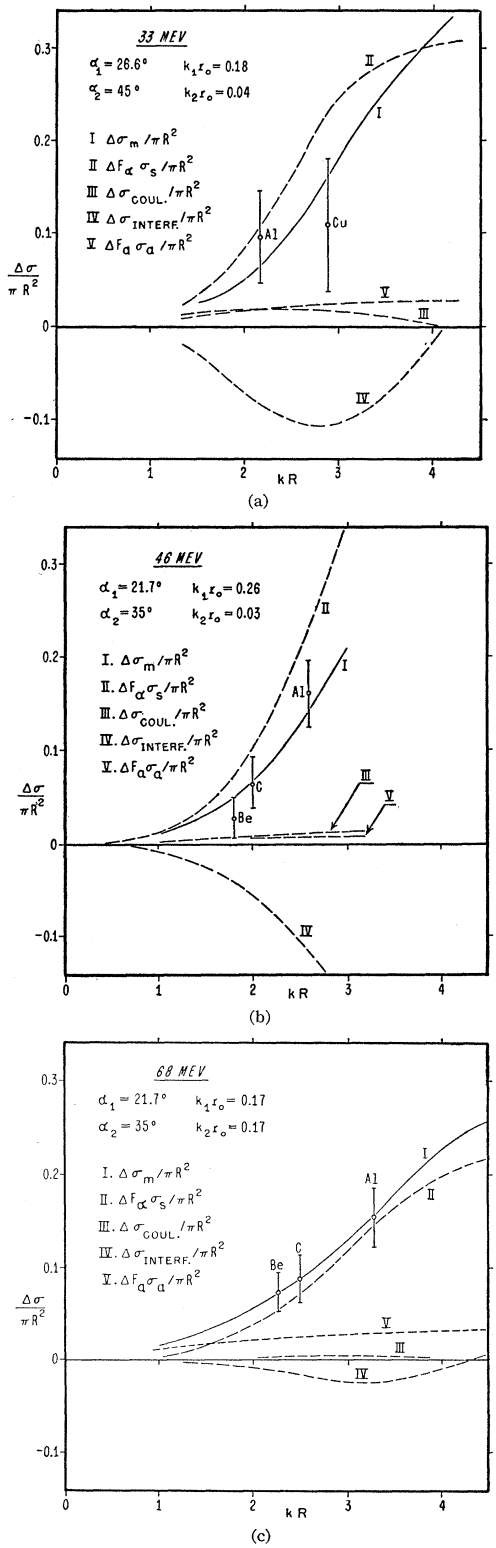

FIG. 8. The measured ring-counter cross sections. The solid curve represents Eq. (3). The Be and C cross sections at 33 Mev were determined in a different geometry and are not shown. They are, however, consistent with the choice of parameters $k_1 r_0$ and $k_2 r_0$.

pression of positive pions at the positively charged nucleus is a second-order Coulomb effect and is treated by means of the correction factor $1+V_c/T_\pi$ as shown in Tables I and II.) It is seen that whereas the total cross section continues to rise with increasing kR, the attenuation cross section rises at first, levels off, and approaches the interaction cross section with increasing kR. This is readily understood in terms of the forward peaking of the diffraction scattering as kR is increased. For the same parameters the ring-counter cross sections, calculated according to Eq. (3), are plotted in Fig. 8. The contributions due to square-well scattering, Coulomb scattering, and Coulomb interference are also shown, as is the estimate of the star-prong effect. The measured ring-counter cross sections, corrected by the factor $1+V_c/T_\pi$, are also plotted in Fig. 8.

Of particular significance is the energy dependence of $k_2 r_0$. Inside the nucleus, the exponential decrease of a pion plane wave intensity is $e^{-2k_2 x}$. Writing $e^{-2k_2 x} = e^{-x/\lambda_a}$, one may interpret λ_a as the mean free path for the interaction of pions in nuclear matter. From the best-fit values of $k_2 r_0$ in Table III, it is seen that the mean free path is strongly energy dependent—decreasing sharply with increasing pion energy. A qualitative explanation of this energy dependence may be found by writing $e^{-2k_2 x} = e^{-N\sigma_n x}$, where N is the nucleon density and σ_n is the cross section for the interaction of pions with a bound nucleon in the nucleus. For a lowest-order perturbation theory calculation using the pseudoscalar pion field with gradient coupling to the nucleon, the free nucleon cross section has a p_π^4/E_π^2 energy dependence, where p_π and E_π are the pion momentum and total relativistic energy. This energy dependence is in agreement with measured total $\pi^+ + p$ cross sections in the energy region of interest here.[15] Thus, neglecting binding effects, $k_2 r_0$ is proportional to the free-nucleon cross section and has a p_π^4/E_π^2 energy dependence that may be written

$$k_2 r_0 = (2\lambda_a/r_0)^{-1} = b(kr_0)^4/\gamma^2, \qquad (4)$$

where $k = p_\pi/\hbar$ and $\gamma = E_\pi/R_\pi$, R_π being the pion rest energy; and b is considered to be a constant. The best-fit values of $k_2 r_0$ in Table III are in agreement with this energy dependence and the value of b is determined to be $0.21_{-0.03}^{+0.04}$.

COMPARISON WITH OTHER DATA

Although Eq. (4) is a satisfactory representation of the energy dependence for $k_2 r_0$ found in this experiment, the fairly large statistical uncertainties do not allow a detailed comparison. The results of this experiment, however, may be combined with the results of other experiments in order to make a more quantitative determination of the energy dependence. There have been several experiments in which the carbon nucleus has been used as a target.[4,5,8] The results for the inter-

[15] S. Leonard and D. Stork, Phys. Rev. **93**, 568 (1954).

action cross section, σ_a, divided by nuclear area and corrected for the Coulomb effect, are shown in Fig. 9. From the cloud-chamber data,[4,5] the interaction cross section was determined by adding the cross sections for stars, stops, and inelastic scattering. The results from the present experiment are also shown, determined by means of the optical model from the values of k_2r_0 in Table III. Similarly, the nuclear emulsion interaction cross sections[1-3] (determined by adding the published cross sections for stars, stops, and inelastic scattering) are shown in Fig. 10. They are divided by the weighted average for πR^2 for nuclear emulsion given by Bradner and Rankin,[3] and they are multiplied by $1\pm V_c/T_\pi$ to correct for the Coulomb effect—suppression of the positive pion wave function (+) and enhancement of the negative pion wave function (−) at the positively charged nucleus.

These cross sections were compared with the results of two methods of wave analysis in which the energy dependence of Eq. (4) was used for k_2r_0. The two methods of wave analysis were the optical model and the partial wave analysis. In the optical model the interaction cross section is independent of k_1r_0. The solid curves in Figs. 9 and 10 are the best fits to the data as determined by the optical model and Eq. (4). The least-squares values of b in Eq. (4) are given in Table IV. In contrast to the optical model, the partial wave analysis requires the specification of k_1r_0 as well as k_2r_0 for determination of σ_a. Two values of k_1r_0 were arbitrarily chosen: $k_1r_0=0$ and $k_1r_0=0.25kr_0$. The latter is in rough agreement with the values of k_1r_0 listed in Table III. The partial wave analysis was carried out for carbon only. The dashed curves in Fig. 9 are the best fits to the carbon data as determined by the partial wave analysis and Eq. (4). The least-squares value of b is given in Table IV, the result being the same for both choices of k_1r_0. At the lower values of kR the curves derived by means of the partial wave analysis coincide with the curve from the optical model. Consequently, equally good agreement with the carbon data may be obtained by either method of wave analysis through the use of Eq. (4) for the energy dependence of k_2r_0. The striking difference is the requirement of mean free paths differing by a factor of almost two—the shorter mean free path for the optical model and the longer mean free path for the partial wave analysis. This difference is presumably due to the different treatment of boundary effects in the two methods.

TABLE IV. Values of b from least-squares fit.

Method of analysis	Source of data	b in Eq. (4)
Optical model	This experiment	$0.21^{+0.04}_{-0.03}$
Optical model	All carbon data (see Fig. 9)	0.26±0.03
Optical model	Nuclear emulsion data for π^+ (see Fig. 10)	0.24±0.04
Optical model	Nuclear emulsion data for π^- (see Fig. 10)	0.36±0.07
Optical model	All of the above data	0.26±0.02
Partial wave analysis	Carbon data only (see Fig. 9)	0.14±0.02

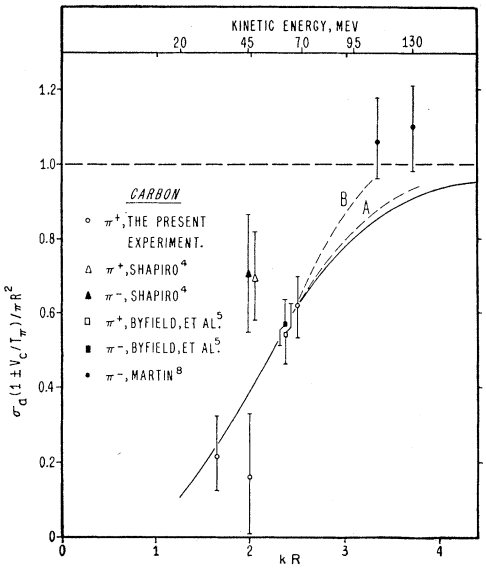

FIG. 9. The pion-carbon interaction cross section. The solid curve is the best fit using the optical model and Eq. (4). The dashed curves are the best fits using the partial wave analysis and Eq. (4). For curve A, $k_1r_0=0$, and for curve B, $k_1r_0=0.25kr_0$.

RELATION TO THE PION-NUCLEON SCATTERING AMPLITUDES

Although the energy dependence given in Eq. (4) was introduced in an *a priori* manner by the assumption

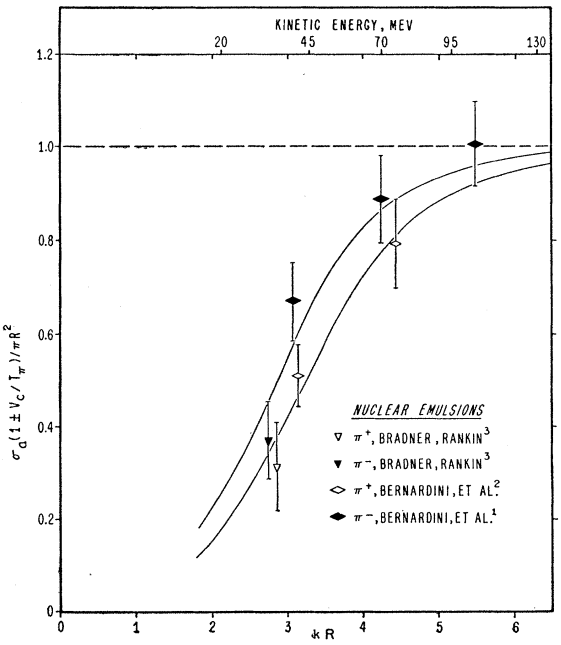

FIG. 10. The pion interaction cross section in nuclear emulsion. The solid curves are the best fits to the negative and to the positive pion data using the optical model and Eq. (4).

that the effect of a bound nucleon is the same as that of a free nucleon, Eq. (4) is to be considered only as an empirically satisfactory representation of the strong energy dependence required for the explanation of the pion-nucleus interaction cross sections by means of a wave analysis. It is desirable, however, to return to a detailed study of the relation between the mean free path for pion interaction in nuclear matter and the interaction of pions with free nucleons. Such a relationship may be established by means of the multiple-scattering theory.

As presented by Lax[16] and applied to nuclei, the multiple-scattering theory considers the nucleus to consist of an ensemble of interaction centers or scatterers representing the nucleons, the ensemble being described by a given probability distribution in the state variables. For the purpose of determining the interaction of an incoming wave with this ensemble, the total wave is found and averaged over the ensemble distribution. The case of a homogeneous medium (uniform spatial density) is considered and the equation

$$k'^2-k^2=4\pi ncf(0^\circ) \tag{5}$$

is found to determine the magnitude of the propagation vector in the medium of the scatterers. The symbols k' and k are the inside and outside wave numbers, n is the density of scatterers given by $n=(4\pi r_0^3/3)^{-1}$, and c is a constant depending upon the correlation between pairs of scatterers. For the present application, c was taken to be unity. $f(0^\circ)$ is the forward scattering amplitude in the case of a free nucleon.

A number of measurements of the angular distribution of pions scattered in liquid hydrogen have been made. The results have been analyzed[17–19] in terms of scattering phase shifts for s and p angular momentum states and for isotopic spin states $\frac{1}{2}$ and $\frac{3}{2}$. From these phase shifts the scattering amplitude for pions incident upon free protons may be found. Using the consequences of charge independence and averaging the scattering amplitudes for equal numbers of protons and neutrons, one finds the forward scattering amplitude required in Eq. (5) for either positive or negative pions, to be

$$\begin{aligned} f(0^\circ)&=a/2+[(1/3)(a+2b)+(\sqrt{2}/3)(a-b)]/2 \\ &=0.901a+0.118b, \end{aligned} \tag{6}$$

where, in the forward direction,

$$a=(\epsilon_3+\epsilon_{31}+2\epsilon_{33})/2ik, \quad b=(\epsilon_1+\epsilon_{11}+2\epsilon_{13})/2ik,$$

and

$$\epsilon_3=e^{2i\alpha_3}-1, \quad \epsilon_{31}=e^{2i\alpha_{31}}-1, \quad \cdots.$$

The notation for the phase shifts, α, is that of Anderson *et al.*[17] The scattering amplitudes a and b are for the isotopic spin states $\frac{3}{2}$ and $\frac{1}{2}$, respectively.

From the sets of phase shifts given for each pion energy, the forward scattering amplitudes were calculated by means of Eq. (6). From Eqs. (1) and (5) the parameters k_1r_0 and k_2r_0 were determined. The interaction mean free path, λ_a/r_0, was calculated from k_2r_0. The results are given in Table V. The forward scattering amplitude is listed in units of r_0 and has been transformed to the laboratory system as is appropriate for the use of Eq. (5). Except at 120 and 135 Mev, the given scattering amplitudes were derived from $\pi^+ + p$ scattering and consequently did not include scattering in the isotopic spin $\frac{1}{2}$ state. However, the contribution of b ($\frac{1}{2}$ isotopic spin state) in Eq. (6) is small. Furthermore, where $\pi^- + p$ ordinary and charge exchange scattering were also measured and the phase shifts for isotopic spin $\frac{1}{2}$ were given (135, 120 Mev),[17] it was found that the magnitude of b was considerably smaller than a. Consequently, the neglect of b for the lower energies should not be serious.

Where the signs of the phase shifts were arbitrary, the signs corresponding to a positive value of k_1r_0 were used. In the case of Bodansky *et al.*,[18] Coulomb interference was a significant factor in their measurements and two different sets of phase shifts were determined by them corresponding to positive and negative interference. The results for both cases are given in Table V. Perry and Angell[19] give two sets of phase shifts (A,B) giving an equally good fit to their data. The results from both sets are shown in Table V. At 120 and 135 Mev, Anderson *et al.*[17] find two equally good sets of phase shifts ("first solution" and "Yang solution"). Both sets give identical results for the forward scattering amplitude.

In Fig. 11 the interaction mean free paths resulting from the above calculation are plotted *versus* pion energy. The uncertainties in the phase shifts are difficult to ascertain and are not given in the references. Consequently, no attempt was made here to determine the uncertainties in the derived mean free paths. The results from the complex-nucleus data are also shown in Fig. 11. The solid curve is from the optical model analysis and corresponds to a value of $b=0.26$ in Eq. (4). The dashed curve is the result of the partial wave analysis with $b=0.14$.

TABLE V. Mean free path from scattering amplitudes.

Source of phase shifts	T_π Mev	$f(0^\circ)/r_0$ (lab.)	k_1r_0	k_2r_0	λ_a/r_0
Anderson *et al.*[a]	135	$4.08+3.94i$	0.600	0.463	1.08
Anderson *et al.*[a]	120	$3.58+2.94i$	0.556	0.370	1.35
Anderson *et al.*[a]	78	$1.94+0.80i$	0.329	0.128	3.9
Anderson *et al.*[a]	53	$3.02+0.43i$	0.072	0.100	5.0
Bodansky *et al.*[b] (−)	58	$-0.33+0.36i$	−0.076	0.080	6.2
Bodansky *et al.*[b] (+)	58	$1.20+0.36i$	0.246	0.068	7.3
Perry, Angell[c] (A)	40	$0.47+0.20i$	0.125	0.051	9.8
Perry, Angell[c] (B)	40	$1.88+0.24i$	0.430	0.047	10.6

[a] See reference 17.
[b] See reference 18.
[c] See reference 19.

[16] M. Lax, Revs. Modern Phys. **23**, 287 (1951).
[17] Anderson, Fermi, Martin, and Nagle, Phys. Rev. **91**, 155 (1953).
[18] Bodansky, Sachs, and Steinberger, Phys. Rev. **90**, 997 (1953).
[19] J. P. Perry and C. E. Angell, Phys. Rev. **91**, 1289 (1953).

DISCUSSION

That the two inside wave numbers could be adjusted to give internal consistency between the four attenuation cross section measurements and the three or four scattering-cross-section measurements at each energy (Figs. 7, 8) indicates the usefulness of the optical model in interpreting the data of this experiment. It has been pointed out[5] that a wave analysis fails to explain the large amount of backscattering found in the nuclear emulsion, and cloud-chamber experiments.[1–6] The experiment of Heckman and Bailey[20] is also pertinent. Le Levier has suggested[21] that a strong repulsive core of the nuclear potential would give rise to backscattering in the wave analysis. Peaslee[22] has attempted to explain these results by adopting an extreme single nucleon scattering model. While these backscatterings are elastic within the rather broad uncertainty of the energy measurements, they may, however, be incoherent scatters in which the pion interacts with a single nucleon rather than with the nucleus as a whole. If so, the large backscattering is expected from the results of measurements of the angular distribution of pion-nucleon scattering.[17–19] In terms of the analysis considered in the present experiment, such events would be included in the interaction cross section, σ_a, rather than the coherent scattering cross section, σ_s.

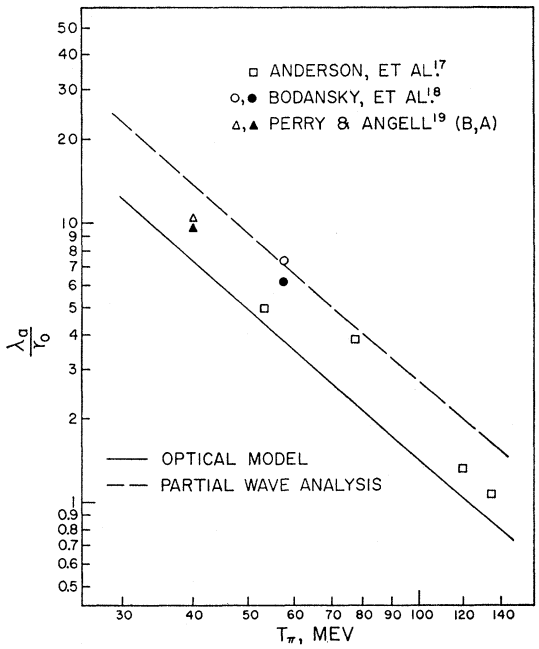

FIG. 11. The mean free path for the interaction of pions in nuclear matter. The points are determined from pion-nucleon scattering phase shifts by means of multiple-scattering theory. The dashed and solid curves are best-fits of Eq. (4) to the pion-nucleus interaction data using the partial-wave analysis and the optical model, respectively.

The strong energy dependence found for the interaction parameter, k_2r_0, was confirmed by comparison of the interaction cross sections reported in other experiments with the cross sections derived by means of the optical model and partial-wave analysis (see Figs. 9 and 10). Equation (4) was found to be a satisfactory representation of the energy dependence required for k_2r_0 in both methods. However, the interaction mean free paths of the partial-wave analysis were found to be nearly twice those determined by the optical model. It is presumed that this discrepancy is caused by the different treatment of boundary effects in the two methods of wave analysis. The optical model neglects reflection and refraction at the nuclear boundary and thus underestimates boundary effects. The partial-wave analysis includes reflection and refraction at the nuclear boundary and thus overestimates boundary effects since the nuclear boundary is probably considerably less abrupt than that in the square-well representation. It is to be expected that a more suitable wave analysis may be found between the two extremes.

A different approach to the interaction mean free path was found in the multiple-scattering theory treatment of the interaction of pions with free nucleons. The results, shown in Fig. 11, are seen to lie generally between the two curves representing Eq. (4) for the two methods of wave analysis. Although this agreement may be to a certain extent fortuitous in view of the approximations in the multiple-scattering theory, the results confirm the strong energy dependence of Eq. (4) and suggest the preference of a method of wave analysis intermediate to the two extremes of the optical model and the partial wave analysis.

It is seen in Fig. 10 that even after correction for Coulomb effects the interaction cross section for negative pions in nuclear emulsion appears to be significantly greater than that for positive pions. It was found in applying the multiple-scattering theory that protons are somewhat more effective in the interaction of positive pions while neutrons are more effective in the interaction of negative pions. However, the neutron excess in nuclear emulsion is insufficient to account for more than a two percent difference in the mean free paths for positive and negative pions. Consequently, the source of the difference in cross sections, if significant, remains in question. It should be noted that the statistical average of the values of b for positive and negative pions in nuclear emulsion is in good agreement with the value for carbon (see Table IV).

Reabsorption is important in the production of pions in complex nuclei. If boundary effects are to be neglected in estimates of reabsorption, it would seem appropriate to use the mean free paths derived on the basis of the optical model. In Fig. 11 it is seen that at

[20] H. H. Heckman and L. Evan Bailey, Phys. Rev. **91**, 1237 (1953).
[21] R. LeLevier, Phys. Rev. **87**, 217 (1952).
[22] D. C. Peaslee, Phys. Rev. **87**, 862 (1952).

low energies the mean free path becomes longer than the average nuclear radius, and thus below about 40 Mev even the largest nucleus should be fairly transparent. Consequently, for low pion energies, the dependence of production cross sections upon atomic mass number, A, may be expected to deviate from the usual $A^{\frac{2}{3}}$ law and, except for Coulomb effects, approach a linear dependence. It should also be noted that Heckman and Bailey[20] find an A dependence for the backscattering of 30-Mev pions.

ACKNOWLEDGMENTS

The encouragement and guidance of Professor Chaim Richman are gratefully acknowledged. The author is indebted to Dr. Stanley Leonard for his assistance throughout a major portion of the experiment. Mr. George Hahn performed the calculations required in the partial wave analysis. Mr. James Vale and the cyclotron crew are to be thanked for their aid in setting up the apparatus and for their efficient operation of the cyclotron.

PHYSICAL REVIEW VOLUME 93, NUMBER 4 FEBRUARY 15, 1954

Elementary Particles and the Lamb-Retherford Line Shift*

LESLIE L. FOLDY† ‡
Case Institute of Technology, Cleveland, Ohio, and Institute for Theoretical Physics, Copenhagen, Denmark
(Received October 26, 1953)

According to the principles of contemporary quantum electrodynamics, the existence of a charged particle field of any kind results in a vacuum polarization contribution to the Lamb-Retherford line shift of an amount proportional to the square of the charge and inversely proportional to the square of the mass of the field particle. On the basis of the present agreement between theory and experiment with respect to the line shift in hydrogen, one may conclude that no singly charged particles of spin-$\frac{1}{2}$ with mass less than four electron masses, other than the electron and positron, can exist without spoiling this agreement. Similar reasoning argues against the existence of singly charged particles of spin-0 with mass less than twice the electron mass. For doubly charged particles these limits are quadrupled. The assumptions involved in these conclusions as well as some experimental evidence are briefly discussed.

THE polarization of the vacuum[1] as a consequence of the existence of the electron-positron field seems now to be a well established phenomenon since it appears to be essential to obtain agreement between experiment[2] and theory[3] for the Lamb-Retherford line shift in the hydrogen atom. To this line shift the vacuum polarization term contributes -27.13 Mc/sec which is some fifty times the discrepancy at present between theory (including fourth order corrections) and experiment.[4] It is characteristic of the theory of the line shift that the existence of any charged particle field which is invariant under charge conjugation will also make a corresponding contribution to the line shift from its vacuum polarization. The contribution of such a particle field is always of the same sign[5] (negative) and, for given spin of the particle, is proportional to the square of the charge and inversely proportional to the square of the mass of the particle. It follows that if one assumes that the present structure of quantum electrodynamics with its renormalization procedure is substantially correct, then one may draw conclusions as to the very existence of other elementary charged particles than those already known, based simply on the present accuracy of agreement of the theory (which neglects the existence of any particles other than electrons and positrons) and experiment for the line shift.

One can see immediately that all well-established charged particles known at present, other than electrons and positrons, will, because of their large mass, make a contribution to the line shift many orders of magnitude below the present difference between theory and experiment[4] which is of the order of 0.5 Mc/sec (= theoretical − observed line shift). However, the existence of elementary singly-charged spin-$\frac{1}{2}$ particles (other than electrons and positrons) with mass less than four electron masses would more th n double the present discordance between theory and experiment. One may thus conclude that the present agreement between theory and experiment argues against the existence of such particles. For doubly-charged particles of spin-$\frac{1}{2}$ this limit of four electron masses would be quadrupled to sixteen electron masses.

For a spin-0 charged particle field[6] theory predicts a vacuum polarization effect which is only one-eighth that

* Publication assisted by National Science Foundation.
† Fulbright and John Simon Guggenheim Memorial Fellow.
‡ On leave for academic year 1953–1954.
[1] E. A. Uehling, Phys. Rev. **48**, 55 (1935).
[2] W. E. Lamb and R. C. Retherford, Phys. Rev. **79**, 549 (1950); **81**, 222 (1951); **86**, 1014 (1952); Triebwasser, Dayhoff, and Lamb, Phys. Rev. **89**, 98 (1953).
[3] R. P. Feynman, Phys. Rev. **74**, 1430 (1948); N. M. Kroll and W. E. Lamb, Phys. Rev. **75**, 388 (1949); J. B. French and V. F. Weisskopf, Phys. Rev. **75**, 1240 (1949).
[4] E. E. Salpeter, Phys. Rev. **89**, 92 (1953).
[5] H. Umezawa and S. Kamefuchi, Progr. Theoret. Phys. Japan **6**, 543 (1951).
[6] R. G. Moorhouse, Phys. Rev. **76**, 1691 (1949); D. Feldman, Phys. Rev. **76**, 1369 (1949).